

Entanglement growth in the dark intervals of a locally monitored free-fermion chain

Giovanni Di Fresco,^{1,*} Youenn Le Gal,^{2,*} Davide Valenti,¹ Marco Schirò,² and Angelo Carollo¹

¹*Dipartimento di Fisica e Chimica "Emilio Segrè",
Group of Interdisciplinary Theoretical Physics, Università degli studi di Palermo,
Viale delle Scienze, Ed. 18, I-90128 Palermo, Italy*

²*JEIP, UAR 3573 CNRS, Collège de France, PSL Research University, 75321 Paris Cedex 05, France*
(Dated: November 22, 2024)

We consider a free fermionic chain with monitoring of the particle density on a single site of the chain and study the entanglement dynamics of quantum jump trajectories. We show that the entanglement entropy grows in time towards a stationary state which display volume law scaling of the entropy, in stark contrast with both the unitary dynamics after a local quench and the no-click limit corresponding to full post-selection. We explain the extensive entanglement growth as a consequence of the peculiar distribution of quantum jumps in time, which display superpoissonian waiting time distribution characterised by a bunching of quantum jumps followed by long dark intervals where no-clicks are detected, akin to the distribution of fluorescence light in a driven atom. We show that the presence of dark intervals is the key feature to explain the effect and that by increasing the number of sites which are monitored the volume law scaling gives away to the Zeno effect and its associated area law.

Introduction – The fluorescence light emitted from a driven atom is characterised by periods of darkness interrupted by random, abrupt periods of brightness, corresponding to quantum jumps between atomic states [1, 2]. These early studies in atomic physics led to the first observations of quantum jumps [3, 4], which have become since then an experimental reality, observed in a variety of platforms in atomic physics, quantum optics and solid-state physics [5]. Quantum jumps also motivated the foundation of the modern theory of quantum trajectories [6–8], describing the physics of a quantum system which is continuously monitored by an external environment [9, 10].

In recent years the effect of quantum jumps and quantum measurements have attracted fresh new interest in the context of open quantum many-body systems [11, 12] and their measurement-induced phase transitions [13–15]. Here the focus is on the entanglement properties of quantum many-body trajectories and how these are affected by the competition between unitary evolution and measurements [16].

The standard setting where this transition has been studied involves the interplay between unitary evolution, described by a many-body Hamiltonian or by a random circuit, and a finite density of local projective measurements [17]. Alternatively, weak-measurement protocols have been also discussed, such as in the quantum jump or quantum state diffusion unravelling of the Lindblad evolution. In these cases one assume every site of the lattice to be exposed to a monitoring stochastic protocol. In all these examples the effect of measurements result in an entanglement transition from a volume-law scaling [18–22], or sub-volume in the case of non-interacting systems [23–42], to an area law where the system is frozen due to the quantum Zeno effect. This elusive criticality is hidden in the fluctuations of the monitoring protocol, while it

remains transparent to the averaged state described by a Lindblad master equation. Experimental investigations of measurement-induced transitions have appeared [43–45] but are plagued by the postselection problem, i.e. the exponential overhead cost in sampling a quantum trajectory associated to a given measurement outcome, even though solutions in certain fine-tuned cases have been proposed [46–48].

In this Letter, we explore the role of monitored dynamics and quantum jumps in a minimal model, where monitoring only occurs locally on a given site of an otherwise free fermionic chain. Local perturbations on quantum many-body systems, i.e. quantum impurities, have been long-known to induce non-trivial effects such as the orthogonality catastrophe [49–52]. Here we show that a non-unitary local monitoring results in a striking growth of entanglement entropy, which slowly saturates to an extensive value scaling with the volume of the subsystem size. This is in stark contrast with both the unitary case and the fully postselected, no-click limit. Therefore our results show that quantum jumps are crucial in generating entanglement. We explain this result by looking at the statistics of quantum jumps, which we reveal to display periods of bunching, interspersed with long dark intervals, similar to the resonance fluorescence of a driven atom. We demonstrate that the presence of these dark periods is the key to extensive entanglement generation and that by monitoring more sites the entanglement generally decreases, recovering the area-law regime expected when each lattice site is monitored.

Model and Monitoring Protocol – We consider a non-interacting 1D fermionic system coupled to a single monitoring device at site j_0 . The fermionic model can be described by the Hamiltonian

$$H_0 = -J \sum_j c_{j+1}^\dagger c_j + h.c. \quad (1)$$

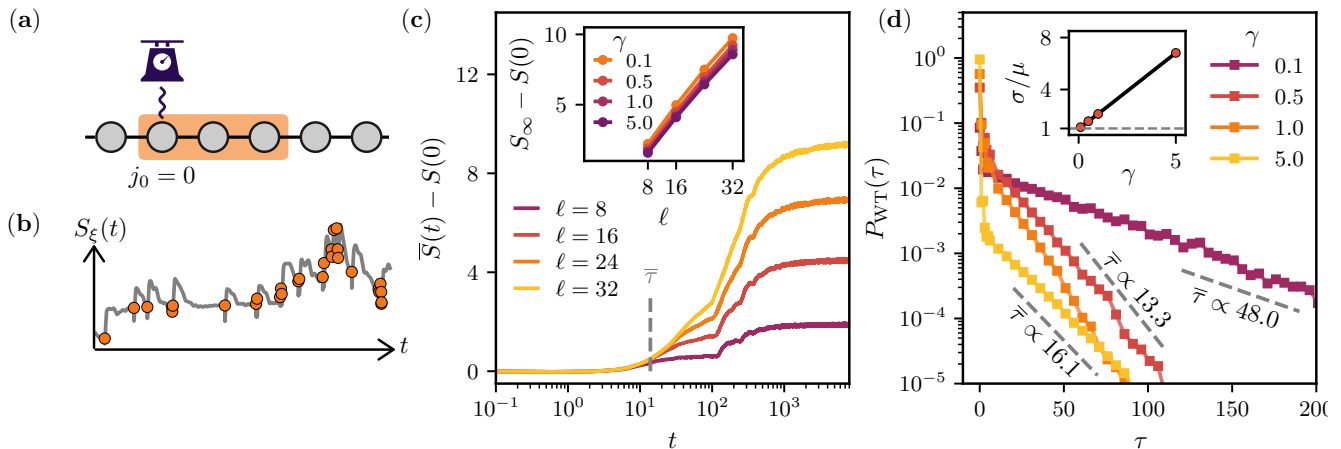


Figure 1. Entanglement dynamics for a locally monitored fermionic chain. (a) Cartoon of the tight-binding chain where the site j_0 is continuously monitored. The yellow region depicts the partition A of size ℓ that we use to compute the bi-partite von Neumann entanglement entropy. (b) Time evolution of the entanglement entropy evaluated along a typical trajectory. (c) Dynamics of the averaged entanglement entropy for a measurement rate $\gamma = 0.5$ and different values of the subsystem size ℓ . In the inset is shown the linear scaling of the long time limit of the entanglement entropy with subsystem sizes ℓ for different measurement rates γ . (d) Waiting time distribution of the jumps for different measurement rates γ . In the inset is depicted the ratio of the standard deviation σ divided by the average μ , characterizing a super-Poissonian distribution for values bigger than one. Parameters: $J = 0.5$, $j_0 = 0$, $L = 128$, $\nu = 1/4$

with L sites and periodic boundary conditions, J being the hopping strength. We consider a monitoring quantum jump protocol where the system wave function evolves randomly in time according to the stochastic Schrödinger equation [6–8, 10]

$$\begin{aligned} \partial_t |\psi\rangle = & -idt \left\{ H - \frac{i}{2} \left(L_{j_0}^\dagger L_{j_0} - \langle L_{j_0}^\dagger L_{j_0} \rangle \right) \right\} |\psi\rangle \\ & + d\xi \left\{ \frac{L_{j_0}}{\sqrt{\langle L_{j_0}^\dagger L_{j_0} \rangle}} - 1 \right\} |\psi\rangle \end{aligned} \quad (2)$$

where $d\xi(t) \in \{0, 1\}$ is an inhomogeneous Poisson increment such that $P(d\xi(t) = 1) = dt \langle \psi(t) | L_{j_0}^\dagger L_{j_0} | \psi(t) \rangle$. The action of the measurement device can be described by one jump operator of the form $L_{j_0} = \sqrt{\gamma} n_{j_0}$ (as depicted in the sketch of Fig. 1 (a)). The first line of Eq. (2) describes the deterministic evolution where unitary dynamics is modified by the measurement back-action, leading to a non-Hermitian Hamiltonian of the form

$$H_{NH} = -J \sum_{j=0}^{L-1} c_{j+1}^\dagger c_j + c_j^\dagger c_{j+1} - i \frac{\gamma}{2} n_{j_0}. \quad (3)$$

This Hamiltonian drives the dynamics in the no-click limit, corresponding to post-selecting the trajectory where no quantum jump arises during the evolution, or in between consecutive quantum jumps. Eq. (3) describes free fermions in an imaginary scattering potential, a problem which has been previously studied [53, 54]. A generic quantum trajectory results in a series of quenched

evolution under the effective non-Hermitian Hamiltonian. For each realisation of this stochastic process, we obtain a trajectory that can be numerically efficiently computed for Gaussian systems [16]. On the other hand, averaging over the full set of trajectories yields a Lindblad master equation dynamics for a free fermion chain subject to a local dephasing process at site j_0 ; a problem addressed in Ref. [54]. In this work we are interested in studying the entanglement structure of quantum trajectories evolving under the protocol described above. Since the evolution conserves the purity and the initial state is chosen to be pure we can consider the von Neumann entanglement entropy defined as $S_\xi(t) = -\text{Tr}_A [\rho_\xi^A(t) \ln \rho_\xi^A(t)]$ where we have introduced a bi-partition A,B (cf Fig. 1 a), with the reduced density matrix $\rho_\xi^A(t) = \text{Tr}_B |\psi_\xi(t)\rangle \langle \psi_\xi(t)|$. In the following, we will discuss in particular the behavior of the entanglement entropy averaged over the measurement noise as

$$\bar{S}(t) = \int \mathcal{D}\xi P(\xi) S_\xi(t). \quad (4)$$

We choose, as an initial state, a Fermi sea with constant filling, ν . This choice makes the no-click evolution a local quench, since it is an eigenstate of the Hermitian part of H_{NH} .

Entanglement properties – We start by discussing the dynamics of entanglement entropy, plotted in Fig. 1c for $\gamma = 0.5$ and different subsystem sizes ℓ . In order to highlight the growth due to the monitoring we subtract the value of the entropy at time $t = 0$, corresponding to the critical Fermi sea. We begin by observing a remarkable

production of entanglement and a threshold behavior. After some initial transient regime, where the entanglement entropy remains close to the initial value, we see a sizeable growth with time and a strong dependence on subsystem size. Furthermore, the entanglement entropy reaches a steady state on a notably slow timescale. While this timescale for free fermions is usually proportional to the sub-system length, here we find it to be much longer and compatible with an exponential scaling [55]. Another remarkable feature is that the steady-state value of the entanglement entropy grows linearly with the subsystem size ℓ , as illustrated in Fig. 1c, i.e. it displays volume law scaling. Unlike typical free-fermion MIPT [23, 25, 32], where the entire chain is monitored, we do not observe an area law scaling regime, even at reasonably large measurement rates γ . Crucially, this is a feature of the local monitoring protocol: indeed, if we increase the number of sites which are monitored we see that the entanglement entropy decreases and the volume law scaling turns into an area-law one [55]. The dramatic effect of a single monitoring protocol on the entanglement dynamics is one of the major results of this work. These results are particularly striking when compared to the no-click limit evolution, corresponding to a local quench by an imaginary scattering potential, but also if compared to the analogous unitary dynamics, i.e. when the quench is realized by a real scattering potential. In both cases indeed the entanglement entropy would quickly saturate to a value independent on sub-system size [55].

This highlights the fact that quantum jumps in our problem play a key role for the entanglement generation. To further understand this point, in the following we will take a closer look to the statistics of quantum jumps.

Statistics of Jumps Waiting times – Looking at a characteristic single shot evolution of the entanglement entropy, plotted in Fig. 1b, already suggests something peculiar occurs in this problem. The way in which quantum jumps are distributed displays two alternating behaviors, characterized by bunching periods and dark periods, respectively. Specifically, the dynamics appears to consist of series of quantum jumps (plotted as orange dots) occurring in close succession (bunching periods), interspersed with long intervals during which the system does not jump, and the dynamics is governed by non-Hermitian evolution (dark periods). This intuition is confirmed by the waiting time distribution (WTD) of quantum jumps, displayed in Fig. 1d, which exhibits two distinct timescales, thereby showing a significant deviation from the typical Poissonian distribution seen in jumps unraveling [56]. Most quantum jumps occur at very short waiting time τ , following a Poissonian distribution. However, we also observe a sizable amount of quantum jumps occurring at a much longer waiting times, giving rise to a statistically significant tails in the distribution. This kind of distribution is known as super-Poissonian, meaning that the ratio of the variance σ to

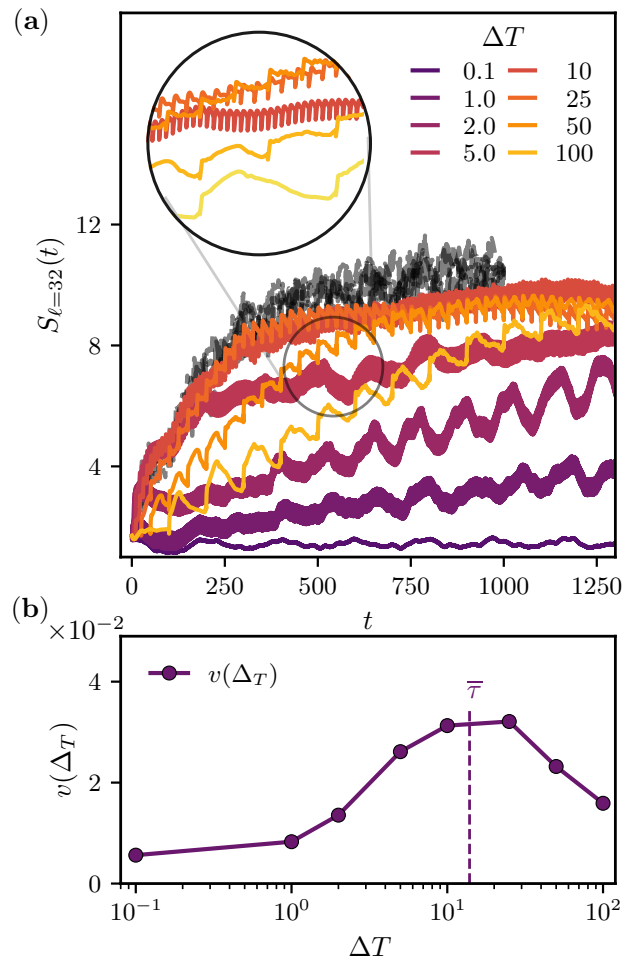


Figure 2. Quantum trajectories at fixed waiting time. (a) Entanglement dynamics of quantum trajectories trajectories where the waiting time is fixed to ΔT . Dark curves represent random typical trajectories and the inset shows a zoom on the dynamics of different waiting times ΔT . (b) Rate of Entanglement growth $v(\Delta T)$ of quantum trajectories as a function of the imposed waiting time. The vertical dashed line indicates the average waiting time $\bar{\tau}$ of the long tail of the full WTD. Parameters: $\gamma = 0.5$, $J = 0.5$, $j_0 = 0$, $L = 128$, $\nu = 1/4$.

the mean μ is greater than one (where a Poissonian distribution has a ratio of one). Super-Poissonian distributions often arise in contexts where events are bunched. We will explain how this distinctive feature plays a key role in generating the observed entanglement dynamics.

Entanglement growth, dark periods and bath disentangling – The emergence of these two time scales in the WTD enables the presence of dark intervals in the monitoring dynamics. The jumps that occur during the bunching periods contribute to the initial exponential decay in the WTD (see Fig. 1 d), while the jumps following the dark periods are responsible for the long tail. An interesting aspect to discern is whether the increase in entanglement can be associated either to the presence of

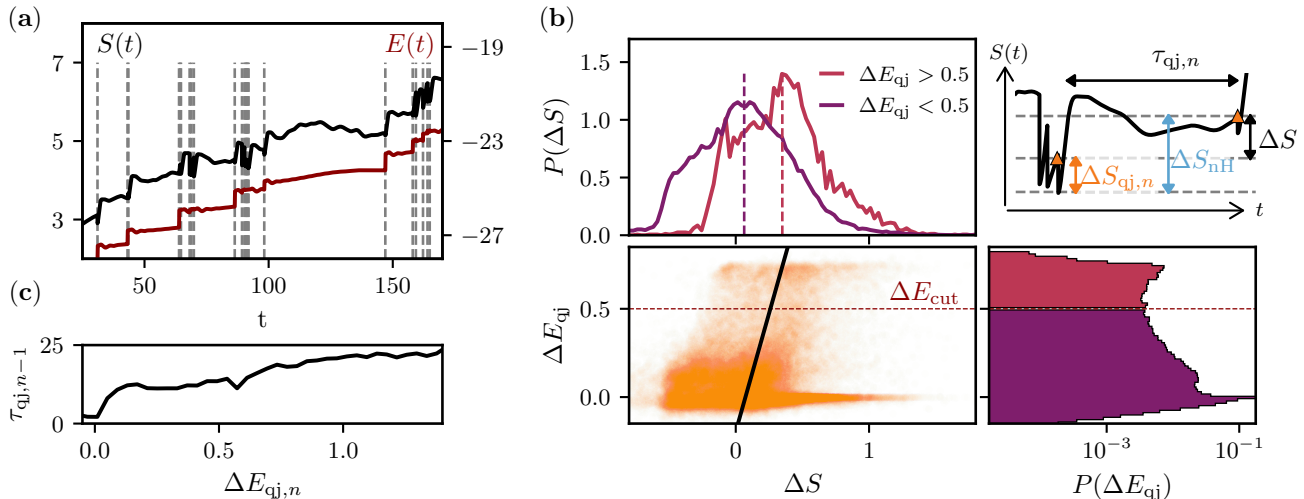


Figure 3. Connection between the tight-binding energy and the entanglement growth. (a) Dynamics of the tight binding energy $E(t)$ (red curve) and of the entanglement entropy $S(t)$ (black curve). The vertical dashed gray lines denote quantum jumps events. (b) Analysis of the correlations between the change of entanglement ΔS and the variation of energy ΔE_{qj} - The top-right panel is a sketch defining the different quantities, thereby $\Delta S_{\text{qj},n}$ denotes the change of entanglement during the n -th quantum jump, and $\tau_{\text{qj},n}$ is the waiting time following the n -th jump. The bottom-left panel shows the correlation between the variation of energy during a quantum jump ΔE_{qj} and the change of entanglement $\Delta S = \Delta S_{\text{qj}} + \Delta S_{\text{nH}}$, happening between the same jumps and the following one (in this expression ΔS_{nH} is the contribution to the entanglement produced in the non-Hermitian evolution between these two jumps, and n is omitted whenever all quantities refer to the same jump event). The dark line represents the linear trend. In top-left panel we show the marginal distribution $P(\Delta S)$ conditioned on the energy variation being larger or smaller than a threshold (dotted line of bottom-left panel). The bottom-right panel shows the marginal distribution $P(\Delta E_{\text{qj}})$. (c) Waiting time in function of the variation of energy $\Delta E_{\text{qj},n}$ occurring in the jump following the wait $\tau_{\text{qj},n-1}$. Parameters: $\gamma = 0.5$, $J = 0.5$, $j_0 = 0$, $L = 128$, $\nu = 1/4$.

bunching or to the long periods during which the measurement device does not click.

We now argue that the key to the extensive volume-law like entanglement growth in our problem of local monitoring consist in these dark periods during which the evolution is driven by a non-Hermitian Hamiltonian, starting however from a different initial state after each random quantum jump. To investigate this, in Fig. 2 we analyze trajectories with fixed waiting times ΔT [57], and we evaluate the entanglement dynamics along them. As we show in panel b, the rate of entanglement growth, $v(\Delta T)$, displays a clear non-monotonic dependence on the fixed waiting time ΔT . Importantly, we see that $v(\Delta T)$ reaches its optimal value when ΔT matches the average waiting time $\bar{\tau}$ observed during the dark intervals (cf. Fig 1d). This analysis shows that the essential factor for achieving significant entanglement growth is the presence of these dark periods. To gain further insight into why long dark periods enable entanglement growth we now look in more details at the statistics of the entanglement entropy changes along a quantum trajectory. This metric was recently introduced to understand the mutual role of non-Hermitian evolution and quantum jumps for entanglement phase transitions [16]. As we show in [55], when applied to our model this analysis reveals that the

net effect of quantum jump events is to decrease the entanglement entropy, while the non-Hermitian evolution is responsible for its growth. Interestingly the entanglement loss due to a jump depends non-monotonously on the length of the waiting time preceding the event [55], suggesting that bunched jumps have less effect than the one happening after a dark period of order $\bar{\tau}$.

Although detrimental for entanglement, quantum jumps play a key role in resetting the state onto which the non-Hermitian evolution will act on, allowing extensive entanglement to be generated. This resetting turns out to be substantial, even though the jump operator acts only on a single site of the system - a kind of orthogonality catastrophe. To understand this point we look at the dynamics of the free fermion energy $E(t) = \langle \psi_\xi(t) | H_0 | \psi_\xi(t) \rangle$ along a quantum trajectory and compare it to the evolution of the entanglement entropy, see Fig. 3a. We observe two qualitatively different kinds of behaviors associated to each quantum jump, depending on whether a large or a small energy variation, ΔE , is seen across the event. The former occurs usually after a long dark period (see Fig. 3c where the waiting time is plotted as a function of the energy change) and is correlated with large change in the entanglement entropy variation between the event and the following one,

$\Delta S = \Delta S_{\text{qj}} + \Delta S_{\text{nH}}$ (see bottom-left panel of Fig. 3b). Indeed, if we now sample the statistics of entanglement entropy changes conditioned on the amount of energy variation, we see two different behaviors (Fig. 3b top-left panel). Most of weak energy variations typically do not affect entanglement entropy, while the large ones induce a finite net increase, corresponding to the histogram $P_{\Delta E_{\text{qj}} > \Delta E_{\text{cut}}}(\Delta S)$ peaked around a finite non-zero value.

We can now understand at least qualitatively the origin of this extensive entanglement production: when a quantum jump hits the monitored site after a long dark period of no-clicks it induces a non-trivial effect across the chain, disentangling part of it and increasing its energy, thus bringing the system far away from equilibrium. As a result, the non-Hermitian evolution which follows this type of events can be considered akin to a global quantum quench, where part of the chain is perturbed and re-entangled rapidly and efficiently, rather than a local one where entanglement entropy growth can be, at best, logarithmic. Out of this balance between loss due to quantum jumps and gain due to entangling evolution, a steady state is eventually reached after a certain number of dark periods. In the no-click evolution, on the other hand, although the dynamics is still driven by the same non-Hermitian Hamiltonian, the initial state is an eigenstate of the free-fermion Hamiltonian. This implies that the perturbation to the state is only due to the measurement back-action (responsible for the non-Hermiticity), whose effect is too local to induce any sizable change in the bulk of the chain. As such it is not surprising that the entanglement production in the no-click limit remains small [55]. This also clarifies why the entanglement production is non-monotonous with ΔT : if we increase ΔT too much, the system remains stuck with the non-Hermitian Hamiltonian in this steady state for too long, slowing down the entanglement production. Our results therefore showcase how local measurements can have dramatic effect on many-body states. Importantly, while our discussion has been focused on the quantum jump protocol the main effect survives also in presence of projective measurements [55].

Conclusions – In this work we have discussed the effect of local on-site monitoring via quantum jumps on a fermionic chain. Remarkably, we have shown that such a local non-unitary perturbation results in a slow growth of entanglement entropy which saturates to a volume law value, in striking contrast to both the unitary case and the no-click limit where only subextensive entanglement can be generated by local perturbations. We have highlighted the key role of quantum jumps and their super-Poissonian WTD in explaining the entanglement production. In particular we have shown that, while quantum jumps decrease the entanglement entropy they also reset the many-body state disentangling the monitored site and its surrounding from the rest of the chain and thus leaving space for the non-Hermitian evolution to produce

entanglement during the long dark intervals. Our results represent one of the simplest yet nontrivial effects due to monitoring, which crucially comes with low overhead in postselection, given the local monitoring and the slow dynamics leading to few quantum jumps. As such, our results could be experimentally verified in quantum simulators with on-site addressing, such as Rydberg arrays [58–60].

Acknowledgements Y.L.G. acknowledges useful discussions with M. Vanhovecke. Authors acknowledge computational resources on the Collège de France IPH cluster. AC acknowledges support from European Union – Next Generation EU through projects: Eurostart 2022 Topological atom-photon interactions for quantum technologies MUR D.M. 737/2021). AC and DV acknowledge PRIN 2022- PNRR no. P202253RLY Harnessing topological phases for quantum technologies; THENCE – Partenariato Esteso NQSTI – PE00000023 – Spoke 2. MS acknowledges funding from the European Research Council (ERC) under the European Union’s Horizon 2020 research and innovation programme (Grant agreement No. 101002955 – CONQUER).

-
- * These two authors contributed equally to the work
- [1] C. Cohen-Tannoudji and J. Dalibard, *Europhysics Letters* **1**, 441 (1986).
 - [2] R. J. Cook and H. J. Kimble, *Phys. Rev. Lett.* **54**, 1023 (1985).
 - [3] J. C. Bergquist, R. G. Hulet, W. M. Itano, and D. J. Wineland, *Phys. Rev. Lett.* **57**, 1699 (1986).
 - [4] W. Nagourney, J. Sandberg, and H. Dehmelt, *Phys. Rev. Lett.* **56**, 2797 (1986).
 - [5] Z. K. Mineev, S. O. Mundhada, S. Shankar, P. Reinhold, R. Gutiérrez-Jáuregui, R. J. Schoelkopf, M. Mirrahimi, H. J. Carmichael, and M. H. Devoret, *Nature* **570**, 200 (2019).
 - [6] M. Ueda, *Phys. Rev. A* **41**, 3875 (1990).
 - [7] J. Dalibard, Y. Castin, and K. Mølmer, *Phys. Rev. Lett.* **68**, 580 (1992).
 - [8] C. W. Gardiner, A. S. Parkins, and P. Zoller, *Phys. Rev. A* **46**, 4363 (1992).
 - [9] M. B. Plenio and P. L. Knight, *Rev. Mod. Phys.* **70**, 101 (1998).
 - [10] H. M. Wiseman and G. J. Milburn, *Quantum Measurement and Control* (Cambridge University Press, Cambridge, England, 2009).
 - [11] A. J. Daley, *Adv. Phys.* **63**, 77 (2014).
 - [12] R. Fazio, J. Keeling, L. Mazza, and M. Schirò, *Many-body open quantum systems* (2024), [arXiv:2409.10300](https://arxiv.org/abs/2409.10300) [quant-ph].
 - [13] A. Nahum, S. Roy, B. Skinner, and J. Ruhman, *PRX Quantum* **2**, 010352 (2021).
 - [14] Y. Li, X. Chen, and M. P. A. Fisher, *Phys. Rev. B* **98**, 205136 (2018).
 - [15] Y. Li, X. Chen, and M. P. A. Fisher, *Phys. Rev. B* **100**, 134306 (2019).
 - [16] Y. Le Gal, X. Turkeshi, and M. Schirò, *PRX Quantum*

- 5, 030329 (2024).
- [17] M. P. Fisher, V. Khemani, A. Nahum, and S. Vijay, *Annu. Rev. Condens. Matter Phys.* **14**, 335 (2023).
- [18] Y. Fuji and Y. Ashida, *Phys. Rev. B* **102**, 054302 (2020).
- [19] O. Lunt and A. Pal, *Phys. Rev. Res.* **2**, 043072 (2020).
- [20] E. V. H. Doggen, Y. Gefen, I. V. Gornyi, A. D. Mirlin, and D. G. Polyakov, *Phys. Rev. Res.* **4**, 023146 (2022).
- [21] B. Xing, X. Turkeshi, M. Schiró, R. Fazio, and D. Poletti, *Phys. Rev. B* **109**, L060302 (2024).
- [22] A. Altland, M. Buchhold, S. Diehl, and T. Micklitz, *Phys. Rev. Res.* **4**, L022066 (2022).
- [23] X. Cao, A. Tilloy, and A. De Luca, *SciPost Phys.* **7**, 024 (2019).
- [24] L. Fidkowski, J. Haah, and M. B. Hastings, *Quantum* **5**, 382 (2021).
- [25] M. Coppola, E. Tirrito, D. Karevski, and M. Collura, *Phys. Rev. B* **105**, 094303 (2022).
- [26] H. Lóio, A. De Luca, J. De Nardis, and X. Turkeshi, *Phys. Rev. B* **108** (2023).
- [27] I. Poboiko, P. Pöpperl, I. V. Gornyi, and A. D. Mirlin, *Phys. Rev. X* **13**, 041046 (2023).
- [28] C.-M. Jian, H. Shapourian, B. Bauer, and A. W. W. Ludwig, (2023), [arXiv:2302.09094](https://arxiv.org/abs/2302.09094).
- [29] M. Fava, L. Piroli, T. Swann, D. Bernard, and A. Nahum, *Phys. Rev. X* **13**, 041045 (2023).
- [30] C. Carisch, A. Romito, and O. Zilberberg, (2023), [arXiv:2304.02965](https://arxiv.org/abs/2304.02965) [quant-ph].
- [31] T. Jin and D. G. Martin, (2023), [arXiv:2309.15034](https://arxiv.org/abs/2309.15034) [quant-ph].
- [32] O. Alberton, M. Buchhold, and S. Diehl, *Phys. Rev. Lett.* **126**, 170602 (2021).
- [33] M. Van Regemortel, Z.-P. Cian, A. Seif, H. Dehghani, and M. Hafezi, *Phys. Rev. B* **126** (2021).
- [34] X. Turkeshi, A. Biella, R. Fazio, M. Dalmonte, and M. Schiró, *Phys. Rev. B* **103**, 224210 (2021).
- [35] T. Botzung, S. Diehl, and M. Müller, *Phys. Rev. B* **104**, 184422 (2021).
- [36] Y. Bao, S. Choi, and E. Altman, *Ann. Phys.* **435**, 168618 (2021).
- [37] X. Turkeshi, M. Dalmonte, R. Fazio, and M. Schiró, *Phys. Rev. B* **105**, L241114 (2022).
- [38] G. Piccitto, A. Russomanno, and D. Rossini, *Phys. Rev. B* **105**, 064305 (2022).
- [39] G. Kells, D. Meidan, and A. Romito, *SciPost Phys.* **14**, 031 (2023).
- [40] A. Paviglianiti and A. Silva, *Phys. Rev. B* **108**, 184302 (2023).
- [41] T. Müller, S. Diehl, and M. Buchhold, *Phys. Rev. Lett.* **128**, 010605 (2022).
- [42] R. D. Soares, Y. L. Gal, and M. Schiró, *Entanglement transition due to particle losses in a monitored fermionic chain* (2024), [arXiv:2408.03700](https://arxiv.org/abs/2408.03700) [cond-mat.stat-mech].
- [43] C. Noel, P. Niroula, D. Zhu, A. Risinger, L. Egan, D. Biswas, M. Cetina, A. V. Gorshkov, M. J. Gullans, D. A. Huse, and C. Monroe, *Nature Phys.* **18**, 760 (2022).
- [44] J. M. Koh, S.-N. Sun, M. Motta, and A. J. Minnich, *Nature Phys.* **19**, 1314 (2023).
- [45] Google AI and Collaborators, *Nature* **622**, 481–486 (2023).
- [46] M. Ippoliti and V. Khemani, *Phys. Rev. Lett.* **126**, 060501 (2021).
- [47] G. Passarelli, X. Turkeshi, A. Russomanno, P. Lucignano, M. Schiró, and R. Fazio, *Phys. Rev. Lett.* **132**, 163401 (2024).
- [48] S. J. Garratt and E. Altman, *PRX Quantum* **5**, 030311 (2024).
- [49] P. W. Anderson, *Phys. Rev. Lett.* **18**, 1049 (1967).
- [50] E. Bettelheim, A. G. Abanov, and P. Wiegmann, *Phys. Rev. Lett.* **97**, 246402 (2006).
- [51] M. Schiró and A. Mitra, *Phys. Rev. Lett.* **112**, 246401 (2014).
- [52] F. Tonielli, R. Fazio, S. Diehl, and J. Marino, *Phys. Rev. Lett.* **122**, 040604 (2019).
- [53] M. Stefanini and J. Marino, *Orthogonality catastrophe beyond luttinger liquid from post-selection* (2023), [arXiv:2310.00039](https://arxiv.org/abs/2310.00039) [cond-mat.stat-mech].
- [54] P. E. Dolgirev, J. Marino, D. Sels, and E. Demler, *Phys. Rev. B* **102**, 100301 (2020).
- [55] Supplemental Materials.
- [56] The statistics of jumps do not always follow a Poissonian distribution throughout the entire dynamics; however, it usually is reached in the steady state. This is not the case here.
- [57] We generate trajectories with fixed jumping times, irrespective of each jumping probability. In principle this same collection of trajectories could have been obtained through post-selection, but it would have been numerically impractical. We stress that the two procedures converge to the same result.
- [58] T. L. Nguyen, J. M. Raimond, C. Sayrin, R. Cortiñas, T. Cantat-Moltrecht, F. Assemat, I. Dotsenko, S. Gleyzes, S. Haroche, G. Roux, T. Jolicoeur, and M. Brune, *Phys. Rev. X* **8**, 011032 (2018).
- [59] B. Ravon, P. Méhaignerie, Y. Machu, A. D. Hernández, M. Favier, J. M. Raimond, M. Brune, and C. Sayrin, *Phys. Rev. Lett.* **131**, 093401 (2023).
- [60] A. Browaeys and T. Lahaye, *Nature Physics* **16**, 132 (2020).

Supplemental Material to ‘Entanglement growth in the dark intervals of a local monitored free-fermion model’

In this Supplemental Information, we discuss:

1. The Entanglement Entropy Dynamics in the No-Click Limit
2. The saturation time for entanglement entropy under quantum jumps
3. The statistics of Entanglement Gain and Losses
4. The dynamics under projective measurements
5. The crossover from single to many monitored sites

ENTANGLEMENT DYNAMICS IN THE NO-CLICK LIMIT

In this section, we examine the entanglement behavior in one specific trajectory of the full jump unraveling: the so-called no-click limit. This is an exponentially rare, deterministic scenario where no clicks occur throughout the evolution. Although the no-click properties may not capture the broader behavior of the full unraveling, they often reveal intriguing aspects that are worth exploring. The no-click evolution is governed by a non-Hermitian Hamiltonian, and understanding its characteristics is valuable for studying the dynamics of the no-click contribution to each trajectory, and hence, of the full system’s dynamics. Furthermore, since our primary focus is on entanglement dynamics, gaining insight into what occurs in the absence of measurement events is essential to gauge the relative performance of click and no-click evolutions.

In this section, we want to emphasize a point already highlighted in the main text: the presence of quantum jumps is the key ingredient that allows our system to generate significant entanglement. To demonstrate this point in Fig. S1(a) we show the evolution of the entanglement entropy for the no-click Hamiltonian defined in Eq.(3) of

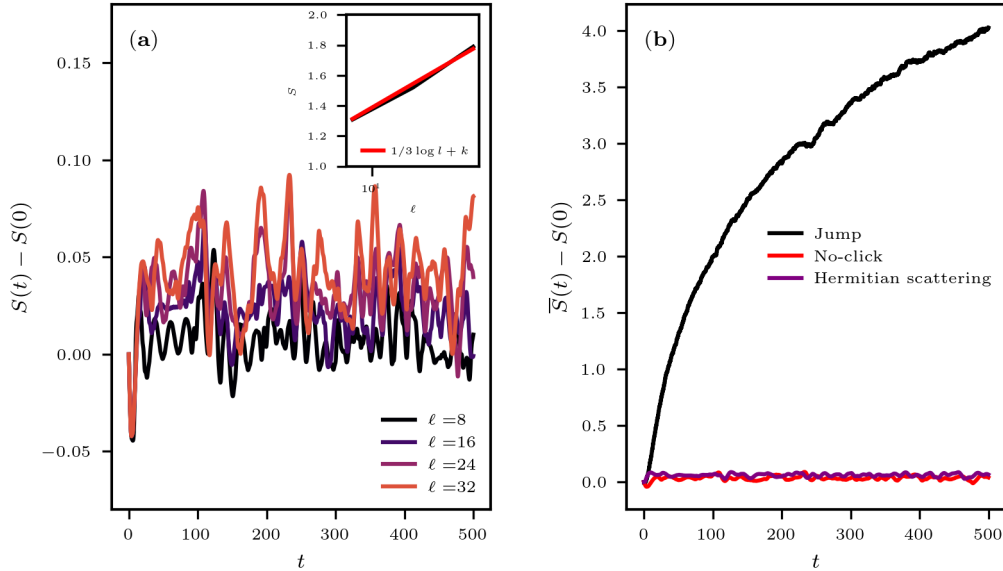


Figure S1. Panel (a): Entanglement entropy as a function of time for different cuts ℓ . The inset shows the scaling of the entanglement with respect to system size. The black solid line represents the numerical data, while the red line indicates the theoretical prediction for the ground state of the free-fermion model. Panel (b): Comparison between the entanglement growth of the no-click scenario (red line) and the averaged entanglement entropy over the full unraveling (black line), as well as the real scattering potential (purple line). Parameters: $J = 0.5$, $\gamma = 0.3$, $j_0 = 0$, $L = 100$, $\nu = 0.25$.

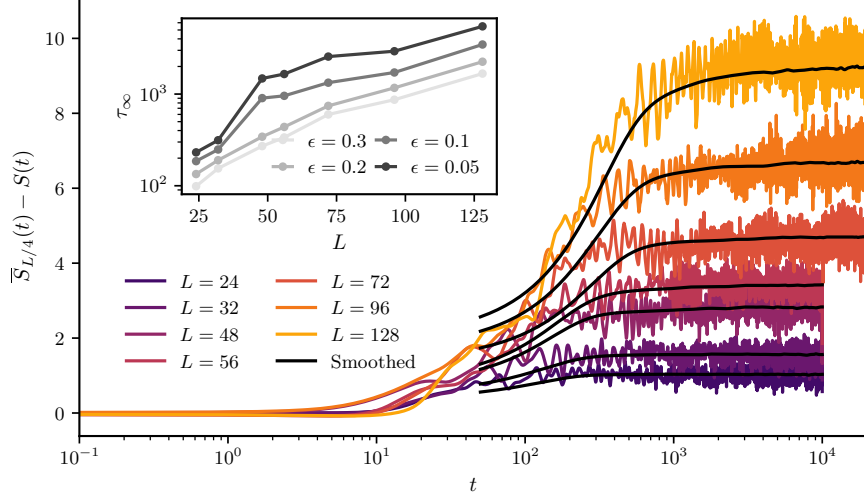


Figure S2. Entanglement entropy dynamics for chains of varying lengths L . The subsystem is for all curves of size $L/4$. The black solid line corresponds to the smoothed dynamics used to determine the saturation time τ_∞ . The inset shows the saturation time τ_∞ scaling with system size L for different ϵ . Parameters: $J = 0.5$, $\gamma = 0.5$, $j_0 = 0$, $\nu = 0.25$.

the main text, for three subsystem sizes ℓ . We see that the entanglement growth is very limited and displays a weak subsystem size dependence that quickly saturates. Note that in this plot we subtract the value at time $t = 0$ to focus on the contribution coming from the time evolution and not from the initial state, a critical Fermi sea with logarithmic scaling of the entanglement entropy which dominates the overall scaling (see inset).

In panel (b) of Fig. S1, we compare the entanglement entropy of the quantum jump trajectories for the same parameters within the same time window, showing the mean entanglement entropy over the jump trajectories alongside the no-click trajectory. As it appears clearly, the curve averaged over the jump trajectories displays significantly higher entanglement content. In panel (b), for the sake of completeness, we also compare these two scenarios with the entanglement that would be generated by a sudden quench of a Hermitian scattering potential $V = \frac{\gamma}{2}n_{j_0}$ (as opposed to the non-unitary scattering $-i\frac{\gamma}{2}n_{j_0}$ of the no-click Hamiltonian in Eq. (3)). This comparison shows that, in this scenario as well, the production of entanglement is negligible.

There are two additional aspects of the non-Hermitian Hamiltonian that we will discuss without explicitly presenting the results. First, it is known that this Hamiltonian has an exceptional point at $\gamma/2J = 1$ [S53]. Interestingly, the entanglement structure, as measured by entanglement entropy, does not seem to be affected by this point, either in no-click trajectories or in the full unraveling (see panel (d) of Fig. 1). The second aspect concerns the role of the impurity position. While its position doesn't alter the qualitative behavior of the system, it does slow down the dynamics.

SATURATION TIME SCALE FOR ENTANGLEMENT ENTROPY

In this section, we analyze the time scale required for the entanglement entropy of our system to reach a steady state, focusing on how the saturation time depends on system size. This process is very slow, which is consistent with the local nature of the monitoring. Getting this saturation time τ_∞ is thus challenging numerically due to the long simulation time required to reach the steady state and also to the sizable number of trajectories needed to reduce sampling noise and thus probe the saturation of entanglement. To this purpose, we compute the entanglement entropy of a system of size L , considering $L/4$ of the chain as a subsystem. By varying the total length, we can observe the relationship between saturation time and system size.

In the main plot of Fig. S2, we show the entanglement entropy dynamics $S_{L/4}(t)$ for chains of different lengths. To attempt to evaluate $\tau_\infty(L)$ we use a Gaussian convolution filter to smoothen the entanglement dynamics. Then we obtain the saturation time as earliest τ_∞ such that $|S(t) - S_\infty| \leq \epsilon$ for all $t > \tau_\infty$ (S_∞ is determined by doing the time integrated average of the late time of the simulation). For each system size the black solid line corresponds to

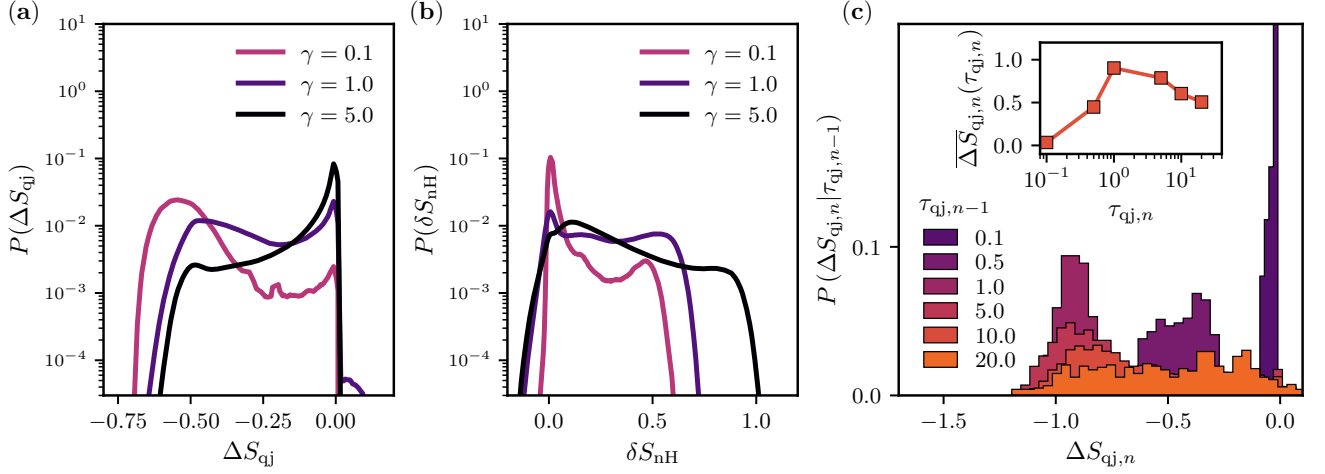


Figure S3. Quantum Jumps Statistics. (a) Statistics of entanglement change due to QJs, $P(\Delta S_{\text{qj}})$. See sketch of Fig. 3 (c) for the definition of the quantities. (b) The corresponding quantity for the non-Hermitian evolution. Here the variation of the entanglement due to the non-Hermitian evolution is renormalized by the waiting time τ such that $\delta_{\text{nH}} = \Delta_{\text{nH}}/\tau$ as done in [S16] (c) The statistics of entanglement change due to QJs, $P(\Delta S_{\text{qj},n}|\tau_{\text{qj},n-1})$, conditioned on the waiting time $\tau_{\text{qj},n-1}$ just before the jump. In the inset the averaged statistics $\overline{\Delta S_{\text{qj},n}(\tau_{\text{qj},n-1})} = \int_{\Delta S_{\text{qj}}} \Delta S_{\text{qj},n} P(\Delta S_{\text{qj},n}|\tau_{\text{qj},n-1})$ is plotted. Parameters: $\gamma = 0.5$, $J = 0.5$, $j_0 = 0$, $L = 128$, $\nu = 1/4$.

the smoothed entanglement dynamics.

The inset shows that the scaling is compatible with an exponential growth of the time τ_∞ to reach the steady state with system size L . We note that, while our numerical analysis does not show a quantitative convergence with ε , the qualitative scaling of τ_∞ with L is compatible with an exponential for every ε . The fact that the time scale for the relaxation of the entanglement is so long, as compared, say, to the unitary dynamics under a Hermitian scattering where the scaling is ballistic, is remarkable. We note that the scaling of the relaxation time with L and the volume-law scaling of the steady-state entanglement appear also to be compatible with the slow dynamics of the entanglement entropy reported in the main text.

STATISTICS OF ENTANGLEMENT GAIN AND LOSS

To understand better the role of quantum jumps and non-Hermitian evolution in the dynamics of our problem we follow Ref. [S16] and study the statistics of entanglement gain and loss along a quantum trajectory. The key idea of this approach is that along a quantum jump trajectory there are two types of evolution, a deterministic one driven by the non-Hermitian Hamiltonian followed by a random quantum jump. Here we monitor the change in entanglement entropy after a quantum jump and in-between them, i.e. during the non-Hermitian evolution, and collect two histograms $P(\Delta S_{\text{qj}})$ and $P(\delta S_{\text{nH}})$ that we plot in Fig. S3(a-b). A remarkable feature of these distributions is the sharpness of their support: quantum jumps appear to always decrease the entropy while non-Hermitian evolution always to increase it. This property is in stark contrast with the case of globally monitored free fermions, where as observed previously [S16] these distributions have tails, implying that a quantum jump has a finite (although small) probability of increase the entanglement entropy.

Moreover, contrary to Ref. [S16]

in this case if we conditioned the QJ distribution on the preceding waiting time, we observe a significant variation of the statistics of entanglement gain due to quantum jumps (See Fig. S3c inset). In particular, the shorter the waiting time is the less effect the jump has on the entanglement (which is consistent with a Zeno effect). When the waiting time increases, the effect on the entanglement also increases until it reaches a maximum. For a longer waiting time the distribution spreads and in average the effect on the entanglement of a QJ diminishes. We retrieve a similar situation to Fig. 2 with a non-monotonous behavior which complements the analysis of the main text.

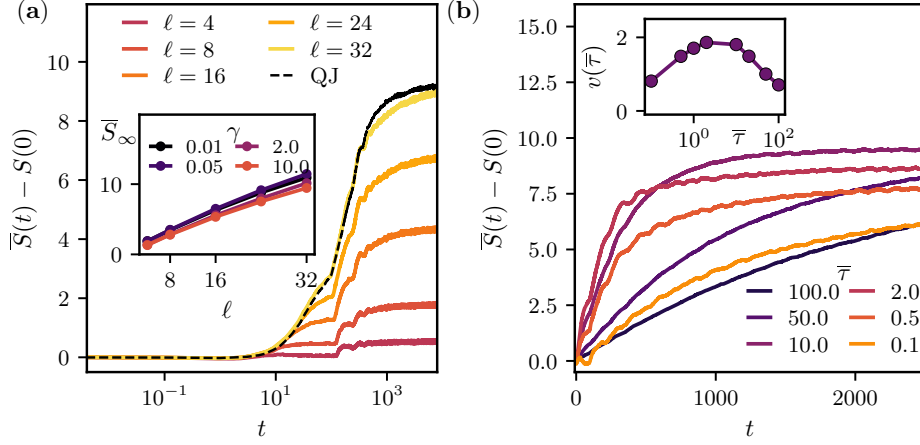


Figure S4. Entanglement Entropy Dynamics under Projective Measurements. (a) Entanglement dynamics for different values of the subsystem size ℓ and $\gamma = 0.5$. The black curves shows the entanglement dynamics in the case of QJs for $\gamma = 0.5$ and $\ell = 32$. In the inset is plotted the long time limit of the entanglement \bar{S}_∞ as a function of the subsystem size ℓ . (b) Entanglement dynamics of $\ell = 32$ and different values of $\gamma = 1/\bar{\tau}$. In the inset we show the growth velocity. Parameters: $J = 0.5$, $j_0 = 0$, $L = 128$, $\nu = 0.25$.

COMPARISON WITH PROJECTIVE MEASUREMENTS

In this section we compare the results for the entanglement entropy obtained in the main text under quantum jumps unraveling with the dynamics under projective measurements. In particular we consider two projectors the site j_0 given by n_{j_0} and $1 - n_{j_0}$ and a unitary evolution with the free-fermion Hamiltonian within the measurement events. The waiting time between the measurement is chosen to follow a Poissonian law of rate γ . In Fig. S4(a) we plot the average entanglement entropy versus time, for different subsystem sizes ℓ , and we find qualitatively a very similar behavior to the results of main text (see dashed line for quantum jumps results). In particular the scaling of the entanglement in the steady state is still linear, compatible with a volume law (see inset). In Fig. S4(b) we plot the short-time dynamics of the entanglement entropy as a function of the average time between measurement $\bar{\tau}$, which in this case is simply given by $1/\gamma$. Interestingly, we see that the slope of the entanglement entropy v depends non monotonically on the average time (see inset), again in agreement with the general picture in the quantum jump case. We stress that in this case changing γ only changes the event distribution in time, thus this strengthens the idea that in the QJs case the non-unitary part is not really important: what really matters is having jumps (here projective measurements) sufficiently spaced in time.

MONITORING A FRACTION OF SITES

In this section, we aim to characterize the transition in the statistical properties of our model from the scenario described in the main text, i.e. a local monitoring, to the standard one discussed in the literature on measurement-induced entanglement transitions, where each site is monitored. To this end, instead of monitoring a single site j_0 , we choose to monitor N_{imp} sites at positions $j_0, \dots, j_{N_{\text{imp}}}$, gradually increasing the number of impurities until they constitute a fraction of the chain length. The results of this analysis are reported in Fig. S5. Panel (a) shows that as we increase the number of monitoring sites, the entanglement entropy transitions from volume scaling to an area law, according to results of [S27]. Interestingly, this transition from volume to area law is reflected in a change in the waiting time distribution of jumps. Panel (b) shows that, as the number of monitoring sites increases, a transition occurs from super-Poissonian to Poissonian behavior. We can easily see it by looking at the ratio μ/σ , which tends to one when increasing the measurement fraction. Additionally, examining the loss and gain distribution of QJs and non-Hermitian evolution, as the number of detectors increases, is instructive (see panels (c) and (d)). In both cases we observe that the asymmetry decreases when N_{imp} increases, which means that we lose the sharpness discussed in Fig. S3. In the case of QJs big negative variation of the entanglement due to jumps are less likely.

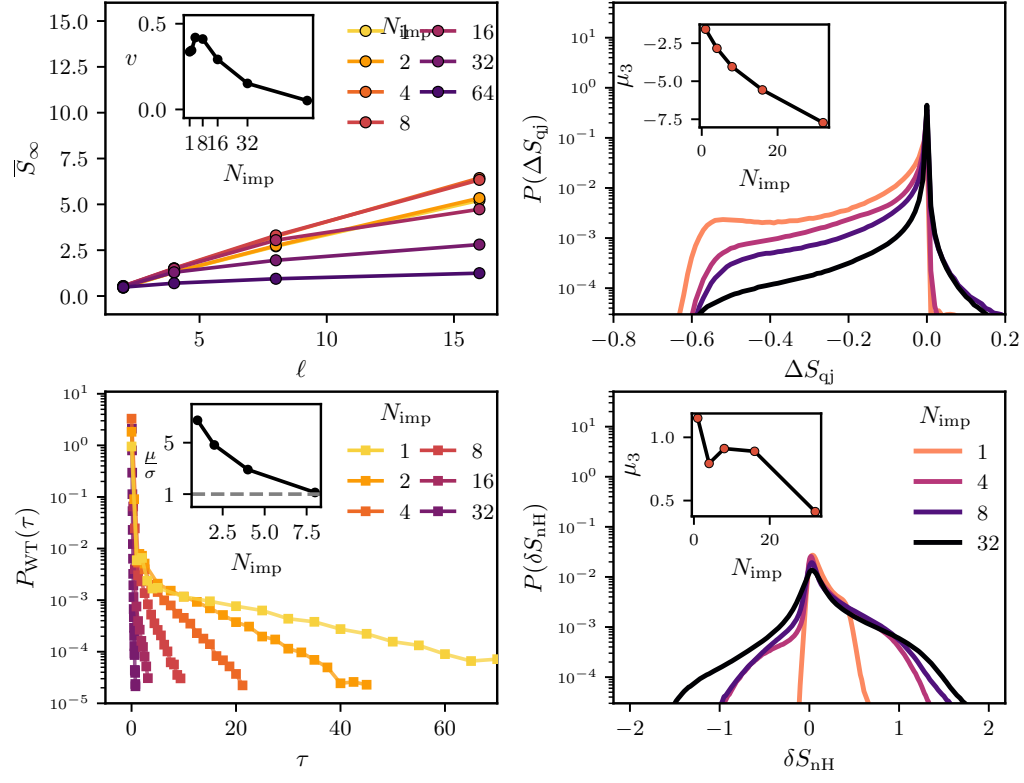


Figure S5. The transition in the statistical properties of the model occurs as the number of monitored sites increases. (a) Entanglement entropy scaling for different number of monitoring sites N_{imp} . The inset shows the coefficient of the linear scaling. (b) Waiting time distribution for different number of monitoring sites N_{imp} . (c) and (d) Distributions of entanglement change $P(\Delta S_{\text{qj}})$ during QJs and non-Hermitian $P(\delta S_{\text{nH}})$. In the insets is plotted the 3rd moment of the distribution, connected with the skewness.